Inter-Research Science Publisher

Aquaculture Environment Interactions
Volume 18:aei00509

Published February 12, 2026
https://doi.org/10.3354/aei00509

Environmental impact of exposed salmon farms: transect reveals matching gradients in seafloor ecosystem structural and functional proxies

Kay Vopel[1,*], David R. Plew[1,2], Michelle N. Simone[1], Adam Davey[3], D. Jeff Ross[3]

[1]School of Science, Auckland University of Technology, Auckland 1142, New Zealand
[2]Earth Sciences New Zealand, PO Box 8602, Christchurch 8440, New Zealand
[3]Institute for Marine and Antarctic Studies, University of Tasmania, Hobart, Tasmania 7001, Australia

ABSTRACT: Exposure of fish pens to strong currents in the open ocean facilitates the dispersion of farm-derived organic-rich solid wastes (faeces, uneaten feed) and thus lessens the effect of waste deposition on the seafloor ecosystem. Quantifying this effect requires tools that can detect deviations in seafloor ecosystem functioning, including trends that, if left unattended, accumulate to cause adverse effects. Here, we demonstrate a spatial gradient in the seafloor O_2 demand, maintained by local deposition of farm-derived organic waste, that could be used as such a tool. To detect this gradient, we measured the *in situ* sediment–seawater O_2 flux with 2 seafloor landers, a benthic chamber lander and an aquatic eddy covariance lander, deployed at 19 sites along a 3000 m transect heading towards a salmon farm in the D'Entrecasteaux Channel, Tasmania, Australia. We found that the seafloor O_2 demand gradually increased within approximately 500 m of the farm from a background level of 220–560 to 1922 µmol m^{-2} h^{-1}. The observed gradient was consistent with a gradient in the biological structure of the seafloor, demonstrated by traditional analyses of benthic macrofaunal assemblages. We discuss how regular monitoring of the seafloor O_2 demand with autonomous benthic landers can support proactive ecosystem-based management of open-ocean fish farms.

KEY WORDS: Open-ocean fish farming · Organic enrichment · Sediment O_2 consumption · Benthic macrofauna

1. INTRODUCTION

Offshore fish farming relies on ecosystem services — the provisioning of environmental conditions for fish growth and the mineralisation of fish farm waste (that is, fish faeces and uneaten food). The importance of the latter service follows because, unlike land-based fish farms, offshore fish farms release their organic waste into the open sea, leaving its decomposition and mineralisation to the pelagic and benthic ecosystems. Whether such practice can be sustainable or not depends on whether farmers have the knowledge, tools, and motivation to operate within the waste-mineralisation capacity of the receiving ecosystem (Bravo & Grant 2018, Hale et al. 2023, Simone & Vopel 2024).

In the nearshore environment, fish farming practices must adhere to environmental constraints, which permit a degree of ecological impact deemed acceptable by regulatory bodies (Wilson et al. 2009, Keeley et al. 2012, Giles et al. 2021). Transitioning this industry to exposed open-ocean locations (Buck et al. 2024, Sclodnick et al. 2024) — a worldwide trend — may mitigate such impact as deeper and more energetic waters can aid in the dispersion and pelagic mineralisation of suspended farm waste, potentially reducing the amount and the biogeochemical reactivity of waste that settles per unit area and time on the seafloor.

Once fish farm waste accumulates on the open-ocean seafloor, the O_2 demand for its aerobic mineralisation will exceed the supply from the bottom seawater. As a result, microbes resort to alternative

*Corresponding author: kay.vopel@aut.ac.nz

Publisher: Inter-Research · www.int-res.com

oxidising agents, most notably the abundant sulphate, leading to the accumulation of sulphides (Fig. 1A) (Bravo & Grant 2018). The (re)oxidation of this and other reduced mineralisation products with O_2 near the sediment surface adds to the biological O_2 demand. The sum of these demands can be measured as the total sediment O_2 demand, a proxy of ecosystem function that quantifies the mineralisation of organic matter by the seafloor ecosystem (Glud 2008).

Both groups of microbial processes — aerobic and anaerobic mineralisation — are profoundly influenced by the composition of sedimentary biota. One commonly used proxy for this composition is the structure of the macrofaunal assemblage. Macrofauna consume and redistribute farm waste, mix porewater solutes, and introduce O_2 into the sedimentary environment (Aller 1994, Meysman et al. 2006, Laverock et al. 2011, Kristensen et al. 2012). Their influence depends on species' identity, abundance, and size, as well as the composition of the species assemblage. A change in this composition can affect the rates of sedimentary solute and particle reaction and transport processes, and vice versa. That is, the capacity of the seafloor ecosystem to assimilate fish waste is a function of its biological structure, which in turn is influenced by the quality and quantity of the organic deposits. Therefore, functional seafloor ecosystem proxies are intimately linked with structural proxies.

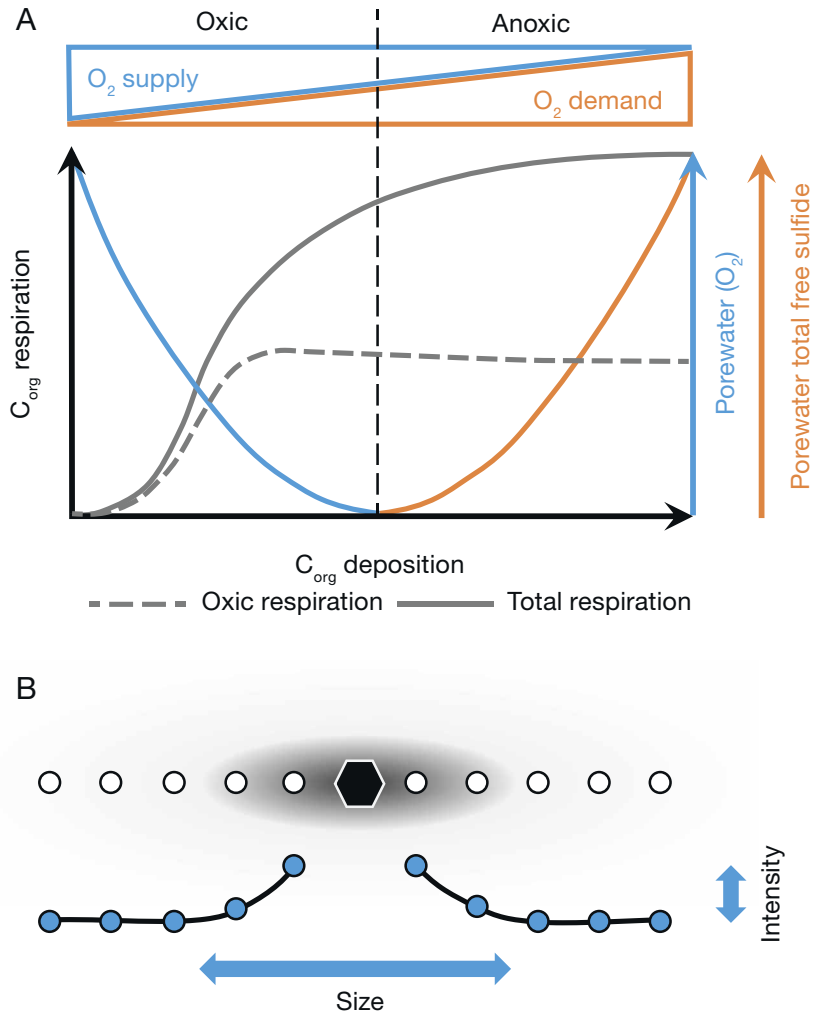

Fig. 1. Conceptual representation of (A) the capacity of seafloor sediment below fish farms to assimilate organic-rich solid waste (adopted from Bravo & Grant 2018), and (B) transect-based monitoring of the organic enrichment footprint (shaded ellipse) of a fish farm (hexagon) in the seafloor ecosystem. C_{org}: organic carbon. In (A), total and oxic C_{org} respiration are represented by the grey solid line and dashed line, respectively, while O_2 and S^{2-} concentrations are represented by the blue and orange lines, respectively. In (B), a series of deployment sites (open symbols) are placed along 2 transects leading towards and away from the farm. At each site, a deployment of an opaque benthic chamber reveals the total chamber O_2 consumption (TCOC; blue symbols). The magnitude of the TCOC, measured at the site closest to the farm, indicates the intensity of the footprint. Sites at which the TCOC exceeds the background TCOC describe the horizontal extension of the footprint. Regular monitoring of these transects reveals if and how the intensity and the horizontal extension of the footprint change over time

Unlike shallow coastal seafloor ecosystems, open-ocean seafloor ecosystems are adapted to low rates of organic matter deposition (Smeaton & Austin 2022). The quantity of waste released by a fish farm in such locations can thus, despite enhanced waste dispersion, exceed the rate at which waste can be oxidised at the seafloor. If so, then this waste accumulates, leading to a shift in the relative contributions of anaerobic and aerobic mineralisation pathways in surface sediment (Glud 2008). For example, organic enrichment may boost anaerobic mineralisation pathways, accompanied by an accumulation of reduced solutes in the sediment porewater (e.g. S^{2-}, Fe^{2+}, Mn^{2+}, NH_4^+), a decrease in sediment porewater oxygenation, accumulation of reduced particulate compounds (e.g. FeS, FeS_2), and possible release of reduced solutes into the bottom seawater (Valdemarsen et al. 2012). Such changes in sediment condition can trigger infauna to emerge from their substrate, decreasing the intensity of bioturbation

and thus further decreasing the capacity of the seafloor ecosystem to mineralise fish waste with O_2. Such positive feedback can eventually transform the seafloor ecosystem into a sulfuretum — an ecosystem dominated by mat-forming, sulphur-oxidising bacteria that explore and control steep, opposing, and overlapping gradients in the concentrations of dissolved O_2 and sulphides at the sediment–water interface.

This shift, which is a natural response of marine sedimentary ecosystems to organic enrichment, is of interest to fish farmers and regulatory and farm management stakeholders because it indicates that the farm operation has exceeded the capacity of the local seafloor ecosystem to mineralise waste. Evidence that such exceedance has happened is usually derived from faunal and biogeochemical analyses of sediment samples, visual inspection of the sediment surface and sediment profile, and other methods (e.g. Kalantzi & Karakassis 2006, Hargrave et al. 2008, 2010, Keeley et al. 2018, 2019, Pochon et al. 2015, Cranford et al. 2017, Simone & Grant 2020). Proactive (anticipatory) ecosystem-based farm management (Bravo & Grant 2018, Simone & Vopel 2024), however, requires methods that can inform farm operations before, not after the fact. The tools that enable such monitoring must (1) be sufficiently sensitive to detect developing deviations in the functioning of the local seafloor ecosystem in real time; (2) be robust to perform under open-ocean conditions; (3) be cost-effective and rapid to support frequent use; and (4) generate quantitative data that enable unambiguous ecological interpretation of trends that, if left unattended, accumulate to cause adverse effects.

Here, we use 2 types of seafloor landers to demonstrate that a fish farm operating in strong currents generates a spatial gradient in the seafloor O_2 demand that can serve as a sensitive proxy for ecosystem function, enabling proactive ecosystem-based farm management (Fig. 1B). We discuss technical aspects of our lander-based measurements and then compare the results with those of parallel structural analyses of the sediment macrofaunal assemblage. Finally, we make suggestions for future technology development that can support the further development and implementation of a lander-based monitoring approach.

2. MATERIALS AND METHODS

2.1. Study site and transect layout

Between 31 May and 10 June 2023, we deployed 2 types of seafloor landers: a benthic chamber lander and an eddy covariance lander, measuring the seafloor O_2 demand at 19 sites placed along a 3 km straight path (hereafter, transect) heading toward Tassal's East of Lippies salmon farm in the D'Entrecasteaux Channel between Bruny Island and the south-east mainland of Tasmania, Australia (Fig. 2). We also collected sediment with a Van Veen Grab at each of 18 sites along this transect, 15 of which coincided with lander deployment sites (see Table 1).

The D'Entrecasteaux Channel connects the estuaries of the Derwent and the Huon Rivers to the Tasman Sea of the South Pacific Ocean. Its hydrodynamics and biogeochemistry are detailed in Herzfeld et al. (2005) and Volkman et al. (2009), respectively. For a comprehensive description of environmental conditions in this area, see Aquenal (2023).

The transect sites were spaced to achieve high-resolution sampling near the farm and broader spatial coverage further away. The first 650 m comprised sites every 50 m, followed by 6 sites spaced 200 m apart, extending the transect 1800 m. Beyond this point, 3 sites were placed at 400 m intervals, reaching a total distance of 3000 m from the farm. This layout was designed to capture the gradient of enrichment near the farm while maximising spatial coverage within the constraints of time and resources. Strong tidal currents and the absence of automatic positioning systems resulted in minor deviations from the planned site locations (see Table 1). For a discussion of the utility of this and other transect-based survey designs, see Foster et al. (2020).

2.2. Benthic chamber incubation

2.2.1. Measurement principle

The benthic chamber lander enclosed a volume of seawater over an area of seafloor sediment and recorded the change in the O_2 concentration within this volume over a period of 2.5 h. The slope of the linear decrease in the O_2 concentration revealed the rate of the total chamber O_2 consumption (TCOC; μmol O_2 m^{-2} h^{-1}). We used the TCOC as a proxy for the total sediment O_2 demand under conditions of darkness, assuming that the O_2 consumption by the bottom seawater would be negligible if this seawater was isolated from the sediment. In other words, the TCOC is the sum of the sediment uptake of O_2 from the bottom seawater and the O_2 consumption caused by oxidation of reduced solutes released by the sediment into the bottom seawater.

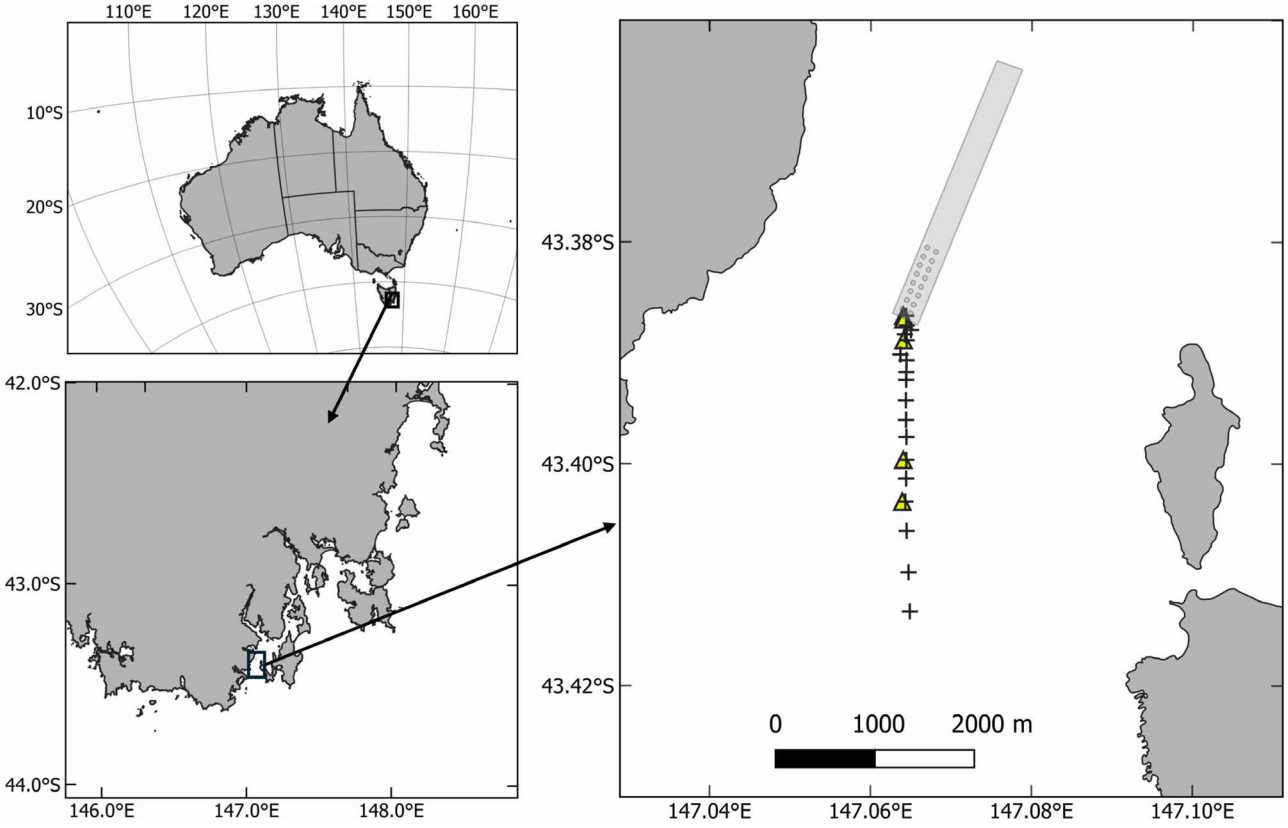

Fig. 2. Location of Tassal's East of Lippies salmon farm lease (grey square) in the D'Entrecasteaux Channel between Bruny Island and the south-east of the mainland of Tasmania, Australia. The lander deployment sites are indicated by + (chamber lander) and triangles (aquatic eddy covariance lander). Circles within the farm lease: location of individual salmon pens at the time of lander deployments

2.2.2. Lander components

We used a Unisense MiniChamber Lander consisting of a stainless steel frame to which a square acrylic chamber (width × length × height: 30 × 30 × 35 cm) was mounted (Fig. 3A). The sides of the chamber were covered with adhesive tape to exclude light. The frame also held a motor-driven syringe water sampler (Fig. 3D), a data logger, a battery pack, an RBR*concerto*^{3} CTD multi-channel logger, and a release mechanism for the chamber lid.

The chamber lid accommodated a motor-driven stirrer (Fig. 3C), a pneumatic silencer, and one port for each of 3 sensors: an Aanderaa optical O_2 optode 4835 (resolution: <0.1 µmol l^{-1}; accuracy: <8 µmol l^{-1}; 63% response time: <30 s), an Aanderaa conductivity sensor 4319B (range: 0–75 mS cm^{-1}; resolution: 0.002 mS cm^{-1}; accuracy: ±0.018 mS cm^{-1}; 90% response time: <3 s), and a Seapoint turbidity sensor (accuracy, ±2% up to 1250 FTU). The built-in temperature sensors of both Aanderaa sensors had a range of −5 to 40°C, resolution of 0.01°C, accuracy of ±0.1°C, and 63% response time of <10 s. The Aanderaa sensors were powered and signals recorded by a Unisense field datalogger. In contrast, the Seapoint sensor was connected to an RBR*concerto*^{3} CTD multichannel logger. The optical design of this sensor confined the sensing volume to within 5 cm of the sensor housing, allowing measurements without errors from chamber wall reflections.

The chamber lid was held open by a magnet, which, on command from the data logger, released the lid. The water-sampling rosette held spring-loaded polypropylene syringes connected with tubing to the sampling ports in the chamber lid. Their spring mechanism was triggered by a rotating, motor-driven actuator arm in the centre of the rosette. We used 2 syringes to inject ~2 × 55 ml of freshwater into the chamber at the end of each measurement period to determine the chamber volume (see below). The pneumatic silencer balanced the pressures inside and outside the chamber as freshwater was added from these syringes.

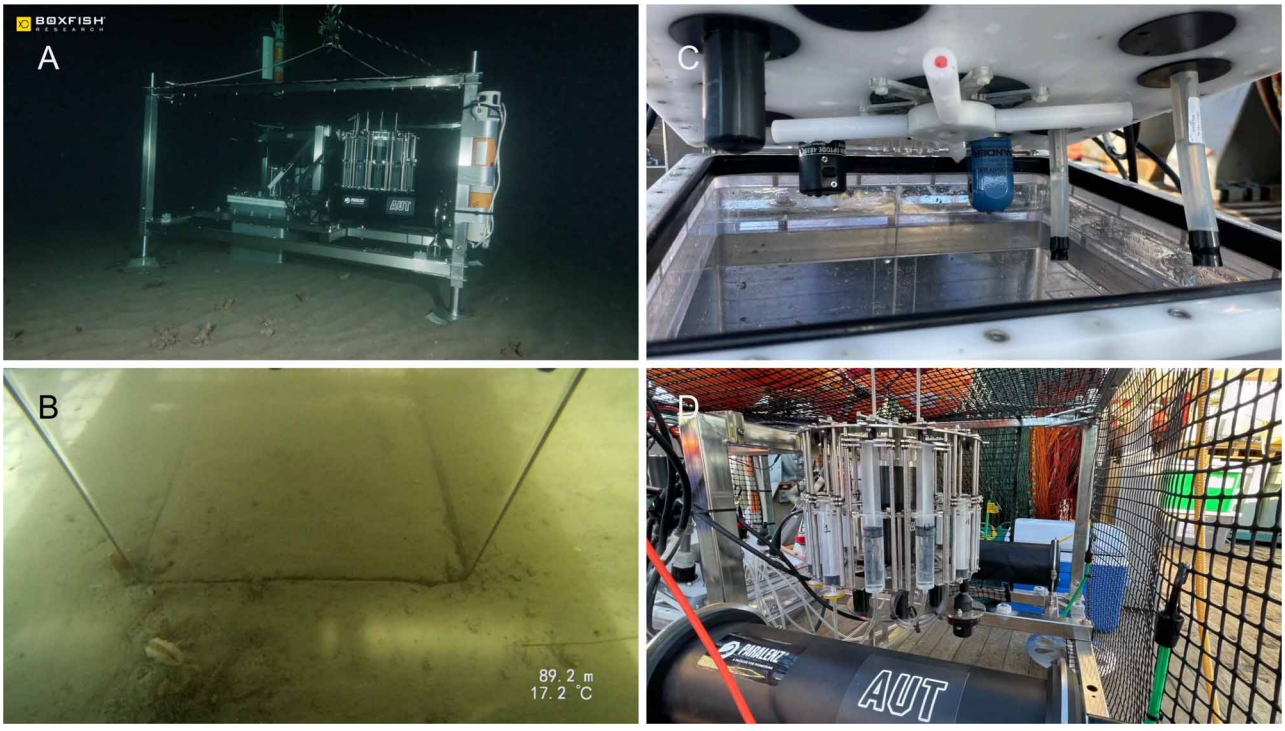

Fig. 3. (A) A Unisense MiniChamber Lander deployed at ~46 m water depth in the D'Entrecasteaux Channel, Tasmania, Australia; (B) a close-up of the lander's clear acrylic chamber deployed at 89 m water depth in Cook Strait, New Zealand; (C) the chamber lid with stirrer in the centre, a Seapoint turbidity sensor, an Aanderaa O_2 Optode 4385, an Aanderaa conductivity sensor (#4319), and 2 pH microelectrodes (Unisense); and (D) the lander's programmable syringe water sampler and data logger in the foreground

2.2.3. Measurement sequence

The lander's datalogger executed a measurement sequence written with a programming tool in the Unisense SensorTrace Suite software package (Table S1 in the Supplement at www.int-res.com/articles/suppl/aei00509_supp.pdf; see below). Included in this package is also the programme 'Logger', which we used to upload measurement routines and download data.

Each measurement sequence lasted about 2.5 h and started with a 10 min trigger delay, which allowed for the deployment of the lander at the seafloor (Table S1). Thereafter, the following settings were executed: stirrer: 80% power (35.3 rpm); data logger frequency: 5 s; and Aanderaa Optode salinity: 35. The optode and conductivity sensors were then started at serial ports 1 and 2, and a delay of 2 min was set to allow the stirrer to disperse sediment particles suspended by the impact of the 4 lander feet. During this delay, the lid of the chamber remained open so that the sensors registered the salinity, temperature, and conductivity of the ambient seawater. Thereafter, the stirrer was stopped and restarted with a 40% power setting (17.2 rpm), and the lid was closed. The data logger then recorded for 143.5 min, after which 2 syringes were released to inject freshwater into the chamber. After another 5 min of recording, both serial ports were closed, and the datalogger and stirrer stopped.

2.2.4. Deployment

We adjusted the height of the lander feet so that after landing on the seafloor, the chamber penetrated the sediment about ~5 cm, enclosing ~27 l of seawater (Fig. 3B). Following the initiation of the measurement sequence (see above), the chamber lander was lowered to the seafloor. We reduced the speed of the winch when the lander approached the seafloor to minimise sediment disturbance during landing and to ensure a straight insertion of the chamber.

2.2.5. Volume of enclosed seawater

The volume of the seawater enclosed by the deployed chamber varied with the depth to which the chamber penetrated the soft sediment, which in turn was determined by sediment physical properties,

lander leg settings, and lander weight. To derive this volume, the lander routine included measurements of the seawater conductivity before and after injection of a known volume of freshwater at the end of each deployment (Table S1). We used these measurements to calculate the change in seawater salinity following Fofonoff & Millard (1983).

The volume of injected freshwater replaced seawater from the chamber; that is, a known mass of salt, through the pneumatic silencer. This resulted in a decrease in chamber water salinity depending on the chamber volume (CV), which can then be calculated as follows:

$$CV = SV \times SBI / (SBI - SAI) \quad (1)$$

where SV (syringe volume) is the volume of injected freshwater, SBI is the salinity before injection, and SAI is the salinity after injection.

2.2.6. Chamber stirring

Previously, we investigated how the speed of the chamber stirrer affects the settling of particles suspended in the enclosed seawater. The goal was to determine a suitable stirrer speed that (1) agitates the seawater in the chamber enough to avoid stratification, and (2) does not resuspend particles that have settled under natural boundary layer conditions. To do so, we deployed the chamber lander on silt–clay sediment in Waihinau Bay, New Zealand. Inspection of the time series of chamber seawater turbidity shown in Fig. 4 revealed that the 2 lowest stirrer speeds, 9.9 and 17.2 rpm, kept the chamber water turbidity between ~2 and ~2.5 NTU, at or slightly above the initial chamber turbidity. An increase to 25.7 and 35.3 rpm after 4 and 6 h, respectively, steeply increased this turbidity. Laboratory observations of particle movement inside the chamber confirmed that even the lowest stirrer speed, 9.9 rpm, caused complete mixing of the enclosed seawater. Guided by these measurements and observations, we decided to use a stirrer speed of 17.2 rpm for all deployments in the D'Entrecasteaux Channel.

2.3. Aquatic eddy covariance

2.3.1. Measurement principle

The aquatic eddy covariance (AEC) method correlates variations in time-series of O_2 concentration and flow velocity measured at a fixed point above the seafloor sediment to derive the sediment–seawater O_2 uptake, hereafter referred to as TOU.

2.3.2. Lander components

We used 3 AEC landers, each consisting of a tripod equipped with instruments measuring velocity, O_2 concentration, temperature, conductivity, and pressure. Near-bed velocities were measured using Nortek Vector acoustic Doppler velocimeters (ADV), with the sample volume (~15 mm in diameter and height) positioned ~0.15 m above the seafloor. A 3-dimensional velocity vector and water pressure were recorded continuously at 16 Hz. A fast response fibre-optic O_2 optode with a sensor tip diameter of <50 µm and 90% response time of <0.15 s (ECO-PSt7, PreSens) was placed 10 mm from the edge of the ADV sample volume. The optode was sampled at 10 Hz, with the 0–5 V output from the amplifier (OXY flux, PreSens) recorded on the Nortek Vector as an analogue input at 64 Hz, and internally averaged down to 16 Hz. Two reference O_2 sensors (MiniDOT, PME) were attached to the legs of each lander (0.15 m above the sediment), logging O_2 and temperature at 1 min intervals. Temperature and conductivity were recorded at 1 min intervals, using a RBR*concerto*^{3} CTD multi-channel logger attached to the lander frames.

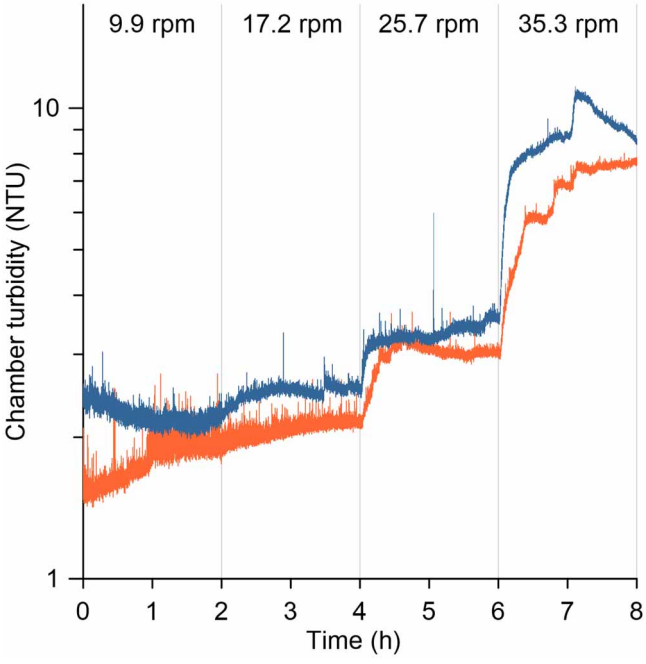

Fig. 4. Waihinau Bay, Waitata Reach, New Zealand, May 2022. Two seawater turbidity (NTU) time-series measured inside the chamber of a Unisense MiniChamber Lander deployed for 8 h at ~32 m water depth (40° 57.055' S, 173° 57.887' E). The speed of the chamber stirrer increased stepwise every 2 h from 9.9 to 35.3 rpm as indicated by vertical lines

2.3.3. Deployment

We deployed the AEC landers for 42–48 h at each of 12 sites but obtained usable data at only 5 sites. The data collection at the remaining 7 sites failed due to damage to the optodes from fish attracted to the flashing optode tip. Prior to deployment, the optode was calibrated with 0 and 100% O_2-saturated seawater. This calibration was repeated at the end of each deployment if the optode was still intact. AEC landers were equipped with acoustic releases with pop-up buoys as a contingency should the surface buoy be lost.

2.3.4. AEC data processing

Eddy covariance data were processed as follows. Output from the optodes was converted to percent saturation using the 2-point calibration described above, and then to concentration (µmol l^{-1}) by calculating the saturation concentration of O_2 in seawater from the salinity and temperature data from the RBR CTD. Oxygen data were corrected for drift using O_2 concentrations measured from the MiniDOT reference sensors. Further processing and flux calculation used the eddy covariance processing software SOHFEA (v.2.0) (McGinnis 2013). Data were averaged down to 8 Hz, and despiked by removing and replacing (by interpolation) O_2 measurements outside of 2 standard deviations from a 300 s running average, and velocity data where vertical accelerations exceeded 0.3 m s^{-2}. A planar rotation was applied to the velocity data to align the vertical velocity component normal to the horizontal streamline velocity (Wilczak et al. 2001, Lorke et al. 2013). Fluxes were then calculated from 15 min bursts, with a 120 s running average used to remove non-turbulent low-frequency fluctuations in vertical velocity and O_2 concentration, and the 2 signals time-shifted by up to 2 s to obtain the maximum flux and correct for sensor response time and the offset between optode and ADV sampling location (McGinnis et al. 2008, Attard et al. 2014). Bursts that contained obvious large fluctuations in O_2 concentration, as identified by large standard deviations relative to other bursts, were discarded. Fluxes were averaged over the entire measurement period.

We used pressure data from the Nortek Vectors to calculate significant wave heights and mean wave periods using pressure time-series for each 15 min burst. We corrected spectra (window size of 2048 data points with 50% overlap) for pressure attenuation using the dispersion relationship after applying a low-pass filter with a cut-off frequency of 0.13 Hz (7.5 s; the shortest wave period that will reach the bed according to linear wave theory). Significant wave heights (H) were calculated as:

$$H = 4(m_0)^{0.5} \quad (2)$$

and mean wave period (T) calculated from:

$$T = (m_0 / m_1) \quad (3)$$

where $m_0 = \int S(f)\,\mathrm{d}f$ and $m_1 = \int fS(f)\,\mathrm{d}f$ are the zeroth and first moments of the wave energy spectra $S(f)$, and f is frequency (Longuet-Higgens 1952, Wiberg & Sherwood 2008).

Near-bed wave orbital velocities (u_w) were estimated from velocity data measured by the Nortek Vectors as follows:

$$u_w = \sqrt{2}\sqrt{\sigma_x^2 + \sigma_y^2} \quad (4)$$

where σ_x and σ_y are standard deviations in x and y velocity components (Wiberg & Sherwood 2008) after applying a 0.5 Hz low-pass filter to reduce turbulence.

2.4. Benthic macrofauna and sediment analyses

We extracted the sediment infauna from a single Van Veen Grab (surface area: 0.0675 m^2) collected at each of 18 sites along the East of Lippies farm transect. All grab samples were wet-sieved to 1 mm and preserved in a 10% formaldehyde–seawater solution in the field. They were then washed and stored in ethanol before being sorted, and the infauna were counted and identified to the lowest possible taxonomic level.

At each site, a sediment subsample of the Van Veen Grab was collected using a 60 ml cut-off syringe (to ~20 mm depth) to evaluate organic carbon and water content. Water content was determined from weight loss after drying the samples at 60°C to a constant weight. The dried sample was then heated to 450°C in a muffle furnace for 4 h and reweighed. Loss of weight on ignition was regarded as organic content, calculated as the percentage dry weight.

2.5. Statistical analyses

We used PRIMER 7 (v.7.0.24) to apply non-parametric multivariate techniques as described in Clarke & Warwick (1994) on log-transformed species abundance data. Such transformation reduces the contributions to similarity by abundant taxa and

therefore increases the importance of the less abundant taxa in the analyses (Clarke 1993). Following this data transformation, we constructed ranked matrices of similarities among the 18 samples using the Bray-Curtis similarity measure, followed by hierarchical cluster analysis (cluster mode: group average) and non-metric multidimensional scaling (nMDS; Kruskal & Wish 1978, Clarke & Green 1988). Finally, we performed SIMPER analyses to evaluate the contribution of individual species to averages of within-group similarities and between-group dissimilarities, and we plotted one *k*-dominance curve for each site to assess within-group and between-group variations in the shape of the cumulative species dominance curve.

3. RESULTS AND DISCUSSION

3.1. Sea conditions

The study site is exposed to ocean swell from the south. Long-period waves (mean period: 10–18 s) reached the seafloor throughout the deployment period, with significant wave heights of up to 1.4 m occurring in the early morning of 4 June 2024, decreasing over subsequent days to 0.2 m by 8 June 2024 before increasing again from midnight 10 June 2024, reaching ~1.0 m by mid-day (Fig. 5A).

Reliable near-bed velocity data are only available from 6 deployments covering 12:30 h on 2 June 2023 to 13:30 h on 6 June 2023. Near-bed currents showed tides flowing northeast–southwest along the axes of the channel, with currents up to 0.10 m s^{-1} at 0.15 m above the bed (Fig. 5B). Fluctuations in near-bed velocity were dominated by wave action, and characteristic near-bed orbital velocities ranged between 0.04 and 0.14 m s^{-1} and trended with wave height (Fig. 5C). At the time of lander deployments, the seawater temperature was ~14°C (Table 1).

3.2. Sediment properties

The upper 10 cm of the sediment was composed of dark greyish brown (10YR/4/2, Munsell soil chart) very fine sand with sparse shell grit. The water content of the sediment was lowest near the farm (~34% wet weight) and highest at the opposite end of the

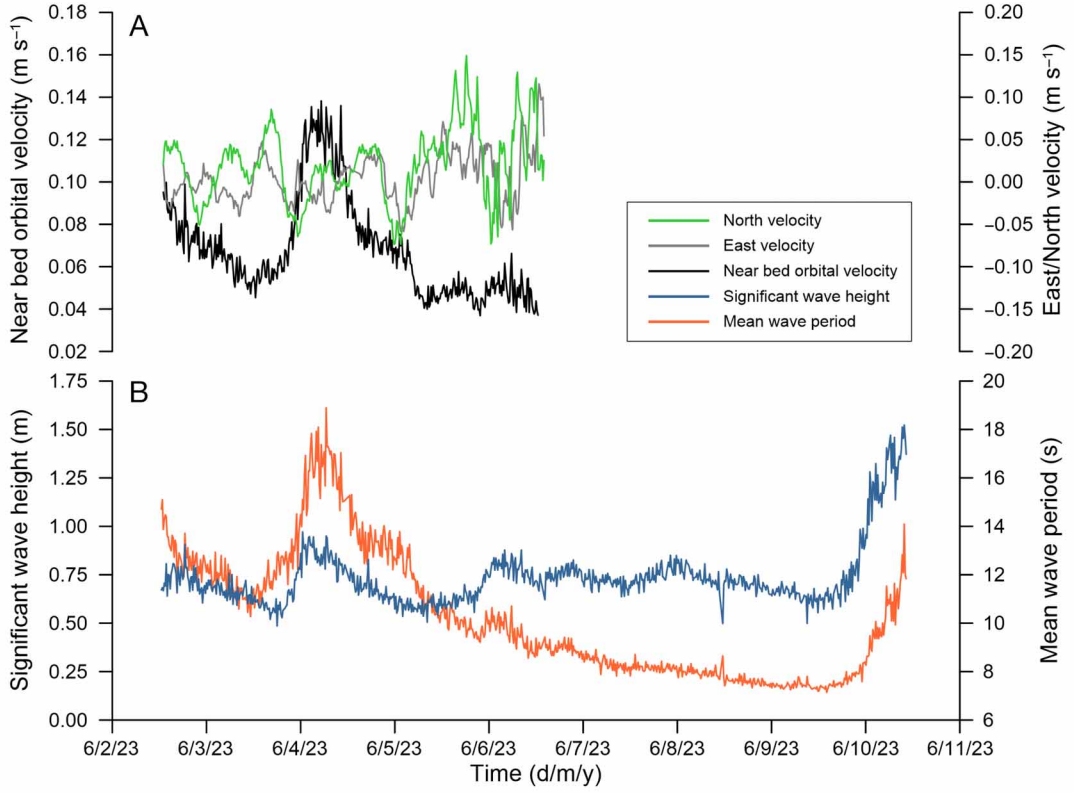

Fig. 5. Hydrodynamic conditions at the East of Lippies salmon farm in June 2023. (A) Near-bed orbital velocity and east and north velocities measured 0.15 m above the sea floor. (B) Significant wave height and mean wave period. Data from nearby deployments at Sites J and I have been combined to create a continuous time series. Note that wave heights and periods are calculated from pressure records, while velocity data are only available for the first half of the experiment

Table 1. Lander deployment and sediment collection sites for the East of Lippies farm transect, D'Entrecasteaux Channel, Tasmania, Australia. Dist.: distance from most southern fish pen; Depth: water depth; Temp.: seawater temperature; SC: species count; IC: individuals count; WC: sediment water content (% wet weight [ww]); OM: sediment organic matter content (% dry weight [dw]). (–) No data collected

ID	Latitude (° S)	Longitude (° E)	Dist. (m)	Depth (m)	Temp. (° C)	SC	IC	WC (% ww)	OM (% dw)
A	43° 23.199′	147° 3.878′	5	47.3	13.6	18	178	34.4	2.8
B	43° 23.218′	147° 3.880′	50	–	–	36	305	34.6	2.7
C	43° 23.251′	147° 3.882′	97	47.4	13.7	43	369	34.9	3.0
D	43° 23.276′	147° 3.913′	190	47.7	13.7	46	492	35.2	3.2
D2	43° 23.300′	147° 3.868′	240	47.7	13.8	48	441	36.9	3.3
E	43° 23.331′	147° 3.881′	290	47.9	13.7	37	422	38.1	3.4
E2	43° 23.356′	147° 3.881′	350	–	–	43	335	39.7	3.9
F2	43° 23.401′	147° 3.891′	430	–	–	35	427	37.5	3.7
F3	43° 23.408′	147° 3.835′	440	47.8	13.7	–	–	–	–
G	43° 23.439′	147° 3.880′	490	48.2	13.7	38	468	36.6	3.9
G2	43° 23.762′	147° 3.877′	560	48.1	13.7	44	372	37.6	3.7
G3	43° 23.504′	147° 3.879′	600	48.3	13.8	43	467	38.1	3.5
H	43° 23.545′	147° 3.878′	680	48.1	13.7	36	412	36.6	3.9
I	43° 23.656′	147° 3.876′	890	48.5	13.7	41	464	38.9	3.8
J	43° 23.762′	147° 3.877′	1000	48.9	13.7	41	484	36.5	3.7
J2	43° 23.854′	147° 3.880′	1250	49.2	13.8	–	–	–	–
K	43° 23.978′	147° 3.879′	1380	49.6	13.7	37	381	37.7	3.5
K2	43° 24.079′	147° 3.878′	1650	49.4	13.8	40	346	38.6	3.7
L	43° 24.204′	147° 3.872′	1850	50.1	13.7	–	–	–	–
M	43° 24.362′	147° 3.882′	2200	49.8	13.8	36	342	39.3	3.5
N	43° 24.586′	147° 3.896′	2600	50.8	13.8	–	–	–	–
O	43° 24.798′	147° 3.906′	3000	50.7	13.8	53	338	41.9	3.7

transect (~42% wet weight; Table 1). The sediment organic matter content ranged between 2.7 and 3.9% dry weight; we measured the lowest values at sites closest to the farm (Table 1).

3.3. Functional ecosystem response: TCOC and TOU

Our transect measurements revealed that the TCOC increased over the distance of the 3000 m-long transect from a background level of 220–560 to 1922 µmol m^{-2} h^{-1} about 5 m next to the most southern fish pen of the East of Lippies farm (Fig. 6). The shape of this spatial gradient suggests that the organic waste released by this salmon farm created a footprint in the seafloor ecosystem function that extended by about 500 m from the most southern fish pen. It appears that this footprint included considerable site-to-site variations in TCOC, suggesting that the waste deposition is patchy, perhaps caused by interactions of fish pen structures with tidal currents in the D'Entrecasteaux Channel.

To put the TCOC measured closest to the fish pens in context, a previous deployment of our lander in

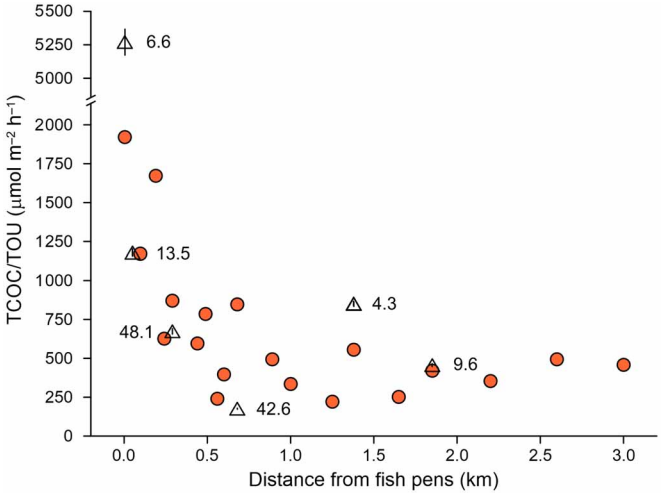

Fig. 6. East of Lippies salmon farm in the D'Entrecasteaux Channel, Tasmania, Australia, in June 2023. The spatial gradient in the seafloor O_2 demand, measured by a benthic chamber lander as total chamber O_2 consumption (TCOC; circles) or by an eddy-covariance lander as total O_2 uptake (TOU; triangles), was derived from consecutive lander deployments along a transect starting 3 km south of the farm in 49 m water depth and heading towards the most southern fish pen in 45 m water depth. Chamber stirrer speed: 17.2 rpm. Vertical lines across triangles: ±SE. Numbers next to triangles indicate deployment period (in hours)

2021 next to a salmon farm in a sheltered bay of Queen Charlotte Sound, New Zealand, revealed 5 times higher TCOC (9547 μmol m^{-2} h^{-1}) in 36 m water depth at a similar temperature of 14.9°C. Other authors, using different methods, reported sediment O_2 consumption rates in sheltered waters of >4000 μmol m^{-2} h^{-1} (Hall et al. 1990, Hargrave et al. 1995, Plew 2019), and reports exist of consumption rates that are an order of magnitude higher (e.g. >24 000 μmol m^{-2} h^{-1}; Findlay & Watling 1997).

AEC measurements of TOU showed good agreement with chamber TCOC measurements (Fig. 6) except for the site closest to the fish pen, where the AEC measurements were 5270 ± 97 μmol m^{-2} h^{-1} (mean ± SE). This higher flux may be due to slight differences in the location of each measurement in an area where the rate of waste deposition increases steeply. In addition, the AEC technique measures fluxes from a larger footprint than the chamber. With the lander configuration used here, the estimated footprint was ~1 m wide and 50–85 m long, with the peak contribution of the flux coming from 2.4–4.4 m upstream of the sensors (Berg et al. 2007, Plew 2019).

We also note that O_2 fluxes derived from AEC are subject to changes in current speeds and background O_2 concentrations (Holtappels et al. 2013) and may lag changes in flux at the seafloor (Rheuban et al. 2014). Fluxes can also vary with flow speed over the tidal cycle (McGinnis et al. 2014, Plew 2019). These effects diminish, however, if fluxes are averaged over sufficient time (Berg et al. 2022), ideally 1 to 2 tidal cycles, depending on whether light reaches the seafloor (Plew 2019).

3.4. Utility of the spatial gradient in seafloor O_2 demand

If the deposition of organic waste released by the East of Lippies farm were to increase, we would expect the seafloor O_2 demand to also increase. The increase in seafloor O_2 demand would be greatest next to the farm, and the gradient of seafloor O_2 demand with distance from the farm would steepen. Furthermore, the distance from the farm at which we can detect an increased O_2 demand relative to the background level may also increase. That is, both the depth (max. demand next to the farm) and size (distance to background level) of the organic enrichment footprint in the seafloor ecosystem would increase.

Alternatively, if farming were to stop, this would gradually erode the gradient until the O_2 demand measured next to the empty fish pens became indistinguishable from the background level. Hence, temporal changes in the gradient of the seafloor O_2 demand can inform about the environmental performance of the fish farm.

A gradient that does not change over time indicates that the release of organic waste from the farm is in balance with the environment's capacity to remove waste via transport and reaction processes. Once such a balance has been observed, environmental managers can then determine if the associated release from the sediment of dissolved reduced products of the microbial waste mineralisation (e.g. ammonium and sulphides) into the bottom seawater is acceptable. Such release extends the influence of the farm beyond the local seafloor ecosystem and may therefore require regulation. The necessary measurements of the fluxes of, for example, ammonium and sulphides may require longer chamber deployments to derive reliable data, but this effort is justified, knowing that such results are not merely a snapshot but representative of a stable balance between waste release and environmental transport and reaction processes.

3.5. Confounding factors and environmental control

Our goal to demonstrate a spatial gradient in the O_2 demand of the seafloor around a fish farm required a series of *in situ* measurements under reproducible environmental conditions. The conditions most important in this regard are those that influence the sediment–seawater O_2 exchange: temperature (benthic metabolic rates), photosynthetically active radiation (PAR; benthic photosynthesis), and bottom layer flow (solute transport regime). This was partly achieved with a benthic chamber that excluded light and controlled the hydrodynamics with a stirrer, so that measurements could be performed consecutively over the course of 11 d, independent of diel and weather-driven fluctuations in PAR (e.g. due to clouds) and bottom layer flow (tides, waves). We note that the intensity of PAR incident at the 47–51 m-deep seafloor, recorded with a planar LICOR sensor mounted on the lander frame, never exceeded 0.02 μmol quanta m^{-2} s^{-1}, suggesting that benthic photosynthesis was unlikely to have contributed to the natural sediment–seawater oxygen flux, and that, therefore, a clear chamber could have been used. However, this may not be the case in other applications.

Although the chamber allowed us to control PAR (exclusion) and chamber water agitation (stirrer set-

ting), a control of seawater temperature was not possible. The data in Table 1 show, however, that seawater temperature did not vary much over the deployment period. For comparison of transect measurements conducted at different times of the year, however, differences in seawater temperature will need to be considered.

AEC and chamber measurements of TOU and TCOC, respectively, showed good agreement, other than immediately adjacent to the farm. The agreement between the 2 methods indicates that the controlled hydrodynamic conditions within the chamber did not alter the O_2 flux.

Waves do not appear to have biased our AEC data. Although horizontal near-bed orbital velocities were significant and comparable in magnitude to tidal currents, the near-bed vertical wave signal was negligible due to the sensor's proximity to the bed (~0.15 m) and the overall water depth (~50 m). Spectral analysis of vertical velocity and O_2 did not show peaks at wave frequencies, supporting this conclusion. This also indicates that the eddy covariance results were not strongly affected by wave action, which can otherwise introduce bias into flux estimates — particularly when time-shift corrections are applied to account for the O_2 sensor's response delay and its offset from the ADV sampling volume (Berg et al. 2015, Reimers et al. 2016, Long 2021).

While not explored in this study, AEC measurements provide a time-series of sediment O_2 fluxes over hours to potentially months (Reimers et al. 2020). While flux estimates are commonly obtained in 15 min increments (Berg et al. 2022), at least 12 h of data are preferred in diurnal tidal flows, or 24 h if significant seafloor primary production occurs, to obtain a reliable estimate of the mean flux (Plew 2019). This, along with the complex data processing required, means that the chamber can more rapidly complete a transect to map the benthic footprint of a farm. However, AEC data could be used to investigate how fluxes vary under different hydrodynamic conditions (tides, weather, light) as well as seasonally (temperature, day length, farm operations). Extended deployments at reference or indicator sites could be used to characterise natural variability and for longer-term monitoring, provided suitable fast-response O_2 sensors with sufficient robustness and life span are selected. In this regard, damage to the optodes caused by fish proved a particular challenge at our study site, resulting in sparse spatial resolution along the length of the transect. Alternative sensors could be considered in future work.

An additional and potentially confounding factor may complicate the interpretation of the transect TCOC measurements: the concentration of resuspended sediment particles in the enclosed chamber seawater. Our measurements inside the chamber shortly after lid closure indeed revealed variable concentrations of suspended particles, shown as initial chamber turbidity in Fig. 7. Such variations may have been caused by differences between individual deployments in the suspended particle load of the seafloor boundary layer. This load will have been determined by the strengths of tidal currents and sea surface conditions at the time of deployment; that is, the height and period of surface waves and associated oscillations in the velocity of the bottom seawater. Inspection of readings taken by the chamber turbidity sensor just seconds before lander touchdown, however, did not confirm a correlation between the boundary layer turbidity and the initial chamber turbidity. Therefore, we assume that the range of initial chamber turbidity readings reflects variations in the degree of sediment disturbance during chamber placement. Such disturbance can result from tidal currents adding a horizontal component to the vertical movement of the lander during touchdown, and wave-induced movement of the deployment vessel at the sea surface,

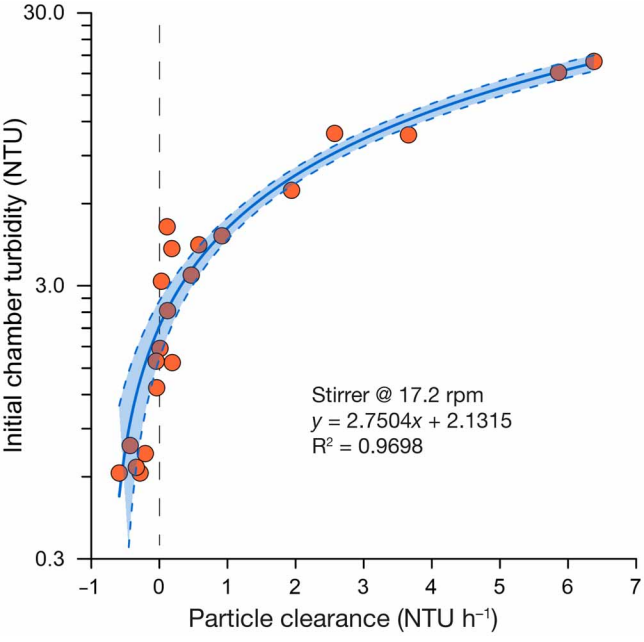

Fig. 7. Initial turbidity and subsequent particle clearance in a benthic chamber deployed at the seafloor of D'Entrecasteaux Channel, Tasmania, Australia, along a transect starting south of Tassal's East of Lippies salmon farm in 49 m water depth and heading towards the most southern pen of this farm in 45 m water depth. Clearance was estimated from the decrease in chamber turbidity during each of 21 chamber deployments, each lasting 3 h. Chamber stirrer speed: 17.2 rpm. Blue solid and dashed lines: linear fit and 95% confidence limits, respectively

preventing a smooth deployment of the chamber. These effects could be reduced if the chamber were deployed after the lander's touchdown, but not simultaneously, or if the lander were freely moving (detached from the vessel) during touchdown.

The closure of the chamber at the beginning of the 2.5 h measurement period isolated the enclosed seawater from the influence of currents and waves, so that the hydrodynamic environment was then defined by the speed of the stirrer. Our recordings showed that a stirrer speed of 17.2 rpm allowed for particle settling during this period, which proceeded at a rate that linearly increased with increasing initial chamber turbidity (Fig. 7). In cases where the initial turbidity was <1 NTU, the stirrer resuspended particles (negative clearance rate). That is, over time, the concentration of particles suspended inside the chamber approached a value defined by sediment granulometry and the stirrer speed. The fit in Fig. 7 indicates that, on average, this value was 2.1 NTU, which is close to the average turbidity of the bottom seawater of 1.2 ± 1.0 NTU (mean ± SD, max.: 4.1; min.: 0.4; n = 21) measured over the 11 d lander deployment period. Other stirrer settings may be required for deployments on much finer sediment, and these could be determined with either a turbidity time-series that includes increasing stirrer speeds, as shown in Fig. 4, or a series of deployments under various sea conditions as shown in Fig. 7.

3.6. Structural ecosystem response: macrofaunal assemblage

The seafloor along the 3000 m transect was populated by a total of 153 macrofaunal species belonging to 94 families and 10 phyla: Arthropoda (classes Malacostraca, Ostracoda, Maxillopoda, Branchiopoda), Mollusca (classes Gastropoda, Bivalvia), Annelida (class Polychaeta), Echinodermata (classes Asteroidea, Ophiuroidea), Platyhelminthes, Sipuncula, Nematoda, Nemertea, Phoronida, and Cnidaria (Table S2). The total count of individuals per grab sample did not exceed 500, and the lowest count of both species and individuals occurred at the site closest to the farm (Table 1).

The hierarchical cluster analysis (cluster mode = group average) shown in Fig. 8A revealed that the species assemblages populating the sediment of the 2 sites 5 and 50 m away from the farm differed significantly from those populating the sediments of the remaining sites. This agrees with the results of our TCOC measurements: the site 5 m away from the farm exhibited the highest O_2 demand. Note that TCOC was not measured at the site 50 m away from the farm.

Furthermore, we found 2 significant groupings of assemblages: one combining sites 97–430 m (64% average similarity) away from the farm, and one combining sites 490–1380 m (69% average similarity) away from the farm (Fig. 8). At a similarity level of 60%, indicated by the vertical dashed line in Fig. 8A, the latter group is extended by the 3 most distant sites (1650, 2200, and 3000 m). This is illustrated in the nMDS plots shown in Fig. 8B. The 2 species contributing the most to the 97–430 m within-group similarity are the amphipods *Byblis mildura* Lowry & Poore, 1985 (12%) and *Ampelisca australis* Haswell, 1879 (11%). Both species were absent at the 2 sites closest to the farm but dominated the remaining sites with an order of magnitude greater abundances. This clustering of sites 97–430 m away from the farm agrees with the measured TCOC gradient. As discussed above, the TCOC data shown in Fig. 6 revealed that the depositional footprint of the fish farm in the seafloor ecosystem extended to about 500 m away from the southern pen, and this observation is supported by the structural analysis of the faunal assemblage.

Interestingly, the faunal assemblage of this 'transition' from the immediate influence of the farm (5 and 50 m) to the background (>430 m) is not only characterised by large site-to-site differences in the TCOC, but also larger site-to-site variations in the structure of the macrofaunal assemblages, as demonstrated by the variations in the shapes of the cumulative dominance of ranked taxa plots shown in Fig. 9. In contrast, sites further away exhibit less variability in both TCOC and the shape of the cumulative dominance plot.

4. CONCLUSIONS

Analyses of the structure of benthic macrofaunal assemblages are a powerful tool for assessment of the effects of organic enrichment on soft-sediment ecosystems, and here, we demonstrated this process again. These analyses are, however, time-consuming and require expertise in the identification of local species. Other indicators of organic enrichment, such as the sediment porewater sulphide content, redox potential, and sediment contents of organic carbon and acid volatile sulphides, are less demanding and widely used, but they still require sediment sampling efforts and laboratory analyses (for an exception, see Wilson & Vopel 2012, 2015).

Here, we used lander-based measurements of the *in situ* seafloor O_2 demand to demonstrate that a fish

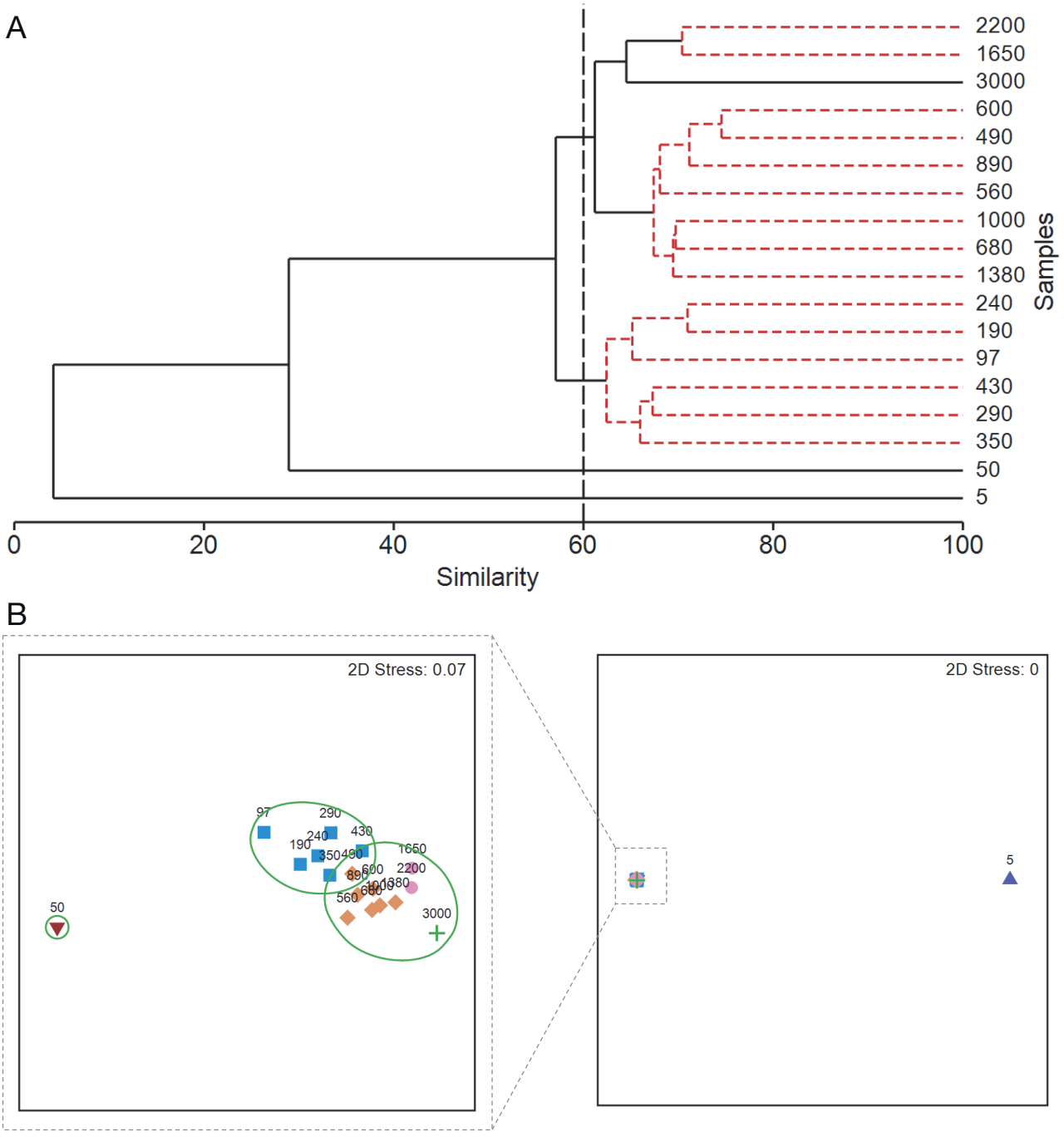

Fig. 8. East of Lippies salmon farm in the D'Entrecasteaux Channel, Tasmania, Australia, in June 2023, showing (A) hierarchical agglomerative clustering and (B) non-metric multi-dimensional scaling of 18 transect sites based on Bray-Curtis similarities of log(x + 1)-transformed species abundances. Numerical site IDs indicate the distance of the site from the most southern fish pen (in m). The symbols and overlay in (B), respectively, indicate statistically significant clusters as determined by a similarity profile (SIMPROF) permutation test (solid horizontal lines in A), and clustering at a 60% resemblance level (vertical dashed line in A)

farm operating in the strong currents of the D'Entrecasteaux Channel maintains a spatial gradient in this demand that could be used as a management tool. We found good agreement between sediment–seawater O_2 fluxes measured by a chamber and fluxes derived from the AEC technique. Overall, the measurements revealed that the influence of the farm on seafloor ecosystem functioning extended to about 500 m be-

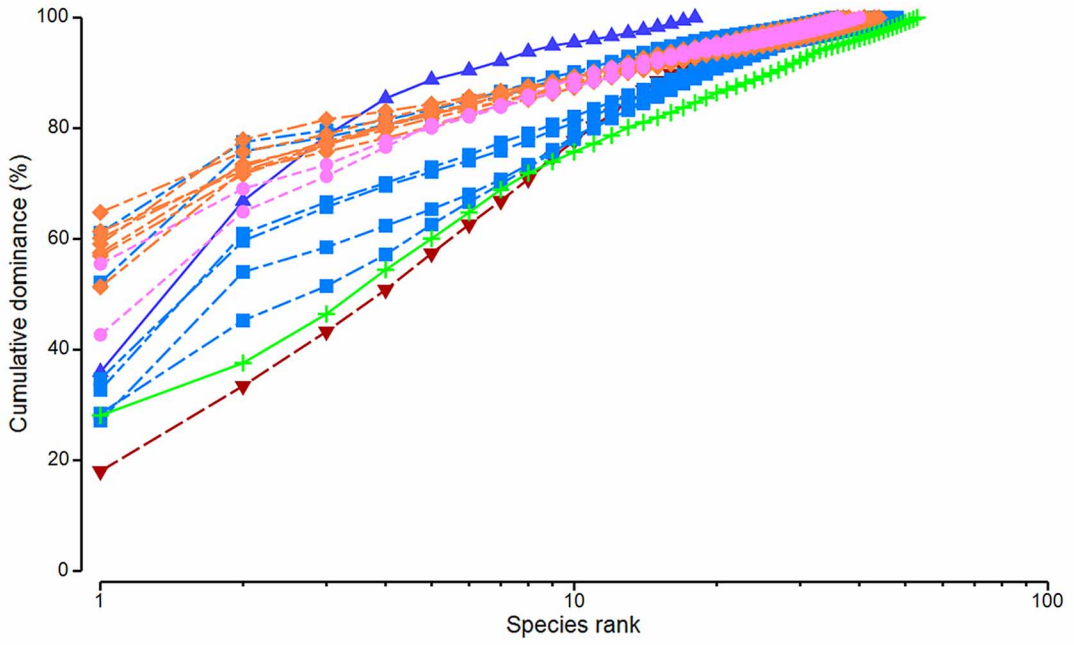

Fig. 9. Cumulative dominance of ranked taxa in the East of Lippies salmon farm in the D'Entrecasteaux Channel, Tasmania, Australia, in June 2023. Symbols match the SIMPROF groups shown in Fig. 8

yond the farm boundary, and this assessment was confirmed by analyses of the macrofaunal species assemblage.

The lander measurements presented here can facilitate frequent assessments of the size and intensity of the fish farm's footprint in the seafloor ecosystem. Unlike analyses of ecosystem structure, they directly quantify the ecosystem function that responds to organic enrichment and thus enable unambiguous ecological interpretation of temporal and spatial trends. Linking this quantitative analysis to a 'limit of acceptable change' (e.g. sediment release of reduced mineralisation intermediates) will provide a proactive (anticipatory) ecosystem-based monitoring tool to manage the environmental performance of open-ocean fish farms.

Acknowledgements. Financial support for this study was provided by the Blue Economy Cooperative Research Centre (BE CRC; project 4.20.004), established and supported under the Australian Government's Cooperative Research Centres Program (grant number CRC-20180101), and the New Zealand Seafood Innovations. We thank the shore teams and boat crews of our industry partner, Tassal, the crews of the NIWA research vessel Ikatere, the team of Marine Aquaculture Contracting, and the field team of the Institute for Marine and Antarctic Studies, University of Tasmania, for assistance and logistical support in the field. Furthermore, we thank Boxfish Robotics for filming the deployment of our landers. Data will be made available on request.

LITERATURE CITED

Aller RC (1994) Bioturbation and remineralization of sedimentary organic matter: effects of redox oscillations. Chem Geol 114:331–345

Aquenal (2023) Broadscale Environmental Monitoring Program — D'Entrecasteaux Channel and Huon Marine Farming Development Plan Sites — Annual Report 2022/2023, July 2023, Report to Salmon Tasmania, 86 pp

Attard KM, Glud RN, McGinnis DF, Rysgaard S (2014) Seasonal rates of benthic primary production in a Greenland fjord measured by aquatic eddy correlation. Limnol Oceanogr 59:1555–1569

Berg P, Roy H, Wiberg PL (2007) Eddy correlation flux measurements: the sediment surface area that contributes to the flux. Limnol Oceanogr 52:1672–1684

Berg P, Reimers CE, Rosman JH, Huettel M, Delgard ML, Reidenbach MA, Özkan-Haller HT (2015) Technical note: time lag correction of aquatic eddy covariance data measured in the presence of waves. Biogeosciences 12:6721–6735

Berg P, Huettel M, Glud RN, Reimers CE, Attard KM (2022) Aquatic eddy covariance: the method and its contributions to defining oxygen and carbon fluxes in marine environments. Annu Rev Mar Sci 14:431–455

Bravo F, Grant J (2018) Modelling sediment assimilative capacity and organic carbon degradation efficiency at marine fish farms. Aquacult Environ Interact 10:309–328

Buck BH, Bjelland HV, Bockus A, Chambers M and others (2024) Resolving the term 'offshore aquaculture' by decoupling 'exposed' and 'distance from the coast'. Front Aquac 3:1428056

Clarke KR (1993) Non-parametric multivariate analyses of changes in community structure. Aust J Ecol 18:117–143

Clarke KR, Green RH (1988) Statistical design and analyses for a 'biological effects' study. Mar Ecol Prog Ser 46: 213–226

Clarke KR, Warwick RM (1994) Change in marine communities: an approach to statistical analysis and interpretation. Natural Environment Research Council, Swindon

Cranford PJ, Brager L, Wong D (2017) A dual indicator approach for monitoring benthic impacts from organic enrichment with test application near Atlantic salmon farms. Mar Pollut Bull 124:258–265

Findlay RH, Watling L (1997) Prediction of benthic impact for salmon net-pens based on the balance of benthic oxygen supply and demand. Mar Ecol Prog Ser 155: 147–157

Fofonoff NP, Millard RC Jr (1983) Algorithms for the computation of fundamental properties of seawater. UNESCO Tech Pap Mar Sci 44:1–53

Foster SD, Hosack GR, Monk J, Lawrence E, Barrett NS, Williams A, Przeslawski R (2020) Spatially balanced designs for transect-based surveys. Methods Ecol Evol 11:95–105

Giles H, Baxter A, Taylor D, Elvines D and others (2021) Best practice guidelines for benthic and water quality monitoring of open ocean finfish culture in New Zealand. New Zealand Aquatic Environment and Biodiversity Report No. 278. Fisheries New Zealand, Wellington

Glud RN (2008) Oxygen dynamics of marine sediments. Mar Biol Res 4:243–289

Hale R, Depree C, Broekhuizen B (2023) Simulating fish farm enrichment and fallowing impacts reveals unequal biogeochemical recovery of benthic variables. Aquacult Environ Interact 15:115–131

Hall POJ, Anderson LG, Holby O, Kollberg S, Samuelsson MO (1990) Chemical fluxes and mass balances in a marine fish cage farm. I. Carbon. Mar Ecol Prog Ser 61:61–73

Hargrave BT (2010) Empirical relationships describing benthic impacts of salmon aquaculture. Aquacult Environ Interact 1:33–46

Hargrave BT, Phillips GA, Doucette LI, White MJ, Milligan TG, Wildish DJ, Cranston RE (1995) Biogeochemical observations to assess benthic impacts of organic enrichment from marine aquaculture in the Western Isles region of the Bay of Fundy, 1994. Can Tech Rep Fish Aquat Sci 2062:1–159

Herzfeld M, Parslow J, Sakov P, Andrewartha JR (2005) Numerical hydrodynamic modelling of the D'Entrecasteaux Channel and Huon Estuary. Aquafin CRC Tech Rep. CSIRO, Hobart

Holtappels M, Glud RN, Donis D, Liu B, Hume A, Wenzhöfer F, Kuypers MMM (2013) Effects of transient bottom water currents and oxygen concentrations on benthic exchange rates as assessed by eddy correlation measurements. J Geophys Res Oceans 118:1157–1169

Kalantzi I, Karakassis I (2006) Benthic impacts of fish farming: meta-analysis of community and geochemical data. Mar Pollut Bull 52:484–493

Keeley N, Forrest B, Crawford C, Macleod C (2012) Exploiting salmon farm benthic enrichment gradients to evaluate the regional performance of biotic indices and environmental indicators. Ecol Indic 23:453–466

Keeley N, Wood SA, Pochon X (2018) Development and preliminary validation of a multi-trophic metabarcoding biotic index for monitoring benthic organic enrichment. Ecol Indic 85:1044–1057

Keeley N, Gillard M, Broekhuizen N, Ford R, Schuckard R, Urlich SC (2019) Best management practice guidelines for salmon farms in the Marlborough Sounds. Part 1. Benthic environmental quality standards and monitoring protocol (Version 1.1 January 2018). New Zealand Aquatic Environment and Biodiversity Report No 219. Prepared for Fisheries New Zealand by the Benthic Standards Working Group. Fisheries New Zealand, Wellington. https://www.mpi.govt.nz/dmsdocument/35610/direct

Kristensen E, Penha-Lopes G, Delefosse M, Valdemarsen T, Quintana CO, Banta GT (2012) What is bioturbation? The need for a precise definition for fauna in aquatic sciences. Mar Ecol Prog Ser 446:285–302

Kruskal JB, Wish M (1978) Multidimensional scaling. Sage University Paper Series on Quantitative Applications in the Social Sciences, No. 07-011. Sage Publications, Newbury Park

Laverock B, Gilbert JA, Tait K, Osborn M, Widdicombe S (2011) Bioturbation: impact on the marine nitrogen cycle. Biochem Soc Trans 39:315–320

Long MH (2021) Aquatic biogeochemical eddy covariance fluxes in the presence of waves. J Geophys Res Oceans 126:e2020JC016637

Longuet-Higgens MS (1952) On the statistical distribution of the heights of sea waves. J Mar Res 11:245–266

Lorke A, McGinnis DF, Maeck A (2013) Eddy-correlation measurements of benthic fluxes under complex flow conditions: effects of coordinate transformations and averaging time scales. Limnol Oceanogr Methods 11:425–437

McGinnis DF (2013) SOHFEA Sulfide-oxygen-heat-flux eddy analysis software package version 2.0, draft user manual. https://sohfea.dfmcginnis.com/

McGinnis DF, Berg P, Brand A, Lorrai C, Edmonds TJ, Wüest A (2008) Measurements of eddy correlation oxygen fluxes in shallow freshwaters: towards routine applications and analysis. Geophys Res Lett 35:L04403

McGinnis DF, Sommer S, Lorke A, Glud RN, Linke P (2014) Quantifying tidally driven benthic oxygen exchange across permeable sediments: an aquatic eddy correlation study. J Geophys Res Oceans 119:6918–6932

Meysman FJR, Middelburg JJ, Heip CHR (2006) Bioturbation: a fresh look at Darwin's last idea. Trends Ecol Evol 21:688–695

Plew DR (2019) Investigating benthic impacts at salmon farms using eddy covariance measurements of benthic oxygen fluxes. Aquacult Environ Interact 11:337–357

Pochon X, Wood SA, Keeley NB, Lejzerowicz F, Esling P, Drew J, Pawlowski J (2015) Accurate assessment of the impact of salmon farming on benthic sediment enrichment using foraminiferal metabarcoding. Mar Pollut Bull 100:370–382

Reimers CE, Özkan-Haller HT, Albright AT, Berg P (2016) Microelectrode velocity effects and aquatic eddy covariance measurements under waves. J Atmos Ocean Technol 33:263–282

Reimers CE, Sanders RD, Dewey R, Noel R (2020) Benthic fluxes of oxygen and heat from a seasonally hypoxic region of Saanich Inlet fjord observed by eddy covariance. Estuar Coast Shelf Sci 243:106815

Rheuban JE, Berg P, McGlathery KJ (2014) Multiple timescale processes drive ecosystem metabolism in eelgrass (*Zostera marina*) meadows. Mar Ecol Prog Ser 507:1–13

Sclodnick T, Chambers M, Costa-Pierce BA, Dewhurst T and others (2024) From 'open ocean' to 'exposed aquaculture': why and how we are changing the standard terminology describing 'offshore aquaculture'. Front Aquac 3: 1428187

Simone MN, Grant J (2020) Visually-based alternatives to sediment environmental monitoring. Mar Pollut Bull 158: 111367

Simone MN, Vopel K (2024) The need for proactive environmental management of offshore aquaculture. Rev Aquacult 16:603–607

Smeaton C, Austin WEN (2022) Quality not quantity: prioritizing the management of sedimentary organic matter across continental shelf seas. Geophys Res Lett 49: e2021GL097481

Valdemarsen T, Bannister RJ, Hansen PK, Holmer M, Ervik A (2012) Biogeochemical malfunctioning in sediments beneath a deep-water fish farm. Environ Pollut 170:15–25

Volkman JK, Thompson P, Herzfeld M, Wild-Allena K and others (2009) A whole-of-ecosystem assessment of environmental issues for salmonid aquaculture. Aquafin Cooperative Research Centre, RC Project 4.2(2). CSIRO Marine and Atmospheric Research, Hobart

Wiberg PL, Sherwood CR (2008) Calculating wave-generated bottom orbital velocities from surface-wave parameters. Comput Geosci 34:1243–1262

Wilczak J, Oncley S, Stage S (2001) Sonic anemometer tilt correction algorithms. Boundary-Layer Meteorol 99: 127–150

Wilson A, Magill S, Black K (2009) Review of environmental impact assessment and monitoring in salmon aquaculture. FAO Fish Aquac Tech Pap 527:455–535

Wilson PS, Vopel K (2012) Estimating the *in situ* distribution of acid volatile sulfides from sediment profile images. Limnol Oceanogr Methods 10:1070–1077

Wilson PS, Vopel K (2015) Assessing the sulfide footprint of mussel farms with sediment profile imagery: a New Zealand trial. PLOS ONE 10:e0129894

Editorial responsibility: Pablo Arechavala Lopez, Esporles, Illes Balears, Spain
Reviewed by: F. Bravo and 2 anonymous referees
Submitted: June 10, 2025; Accepted: October 24, 2025
Proofs received from author(s): February 2, 2026